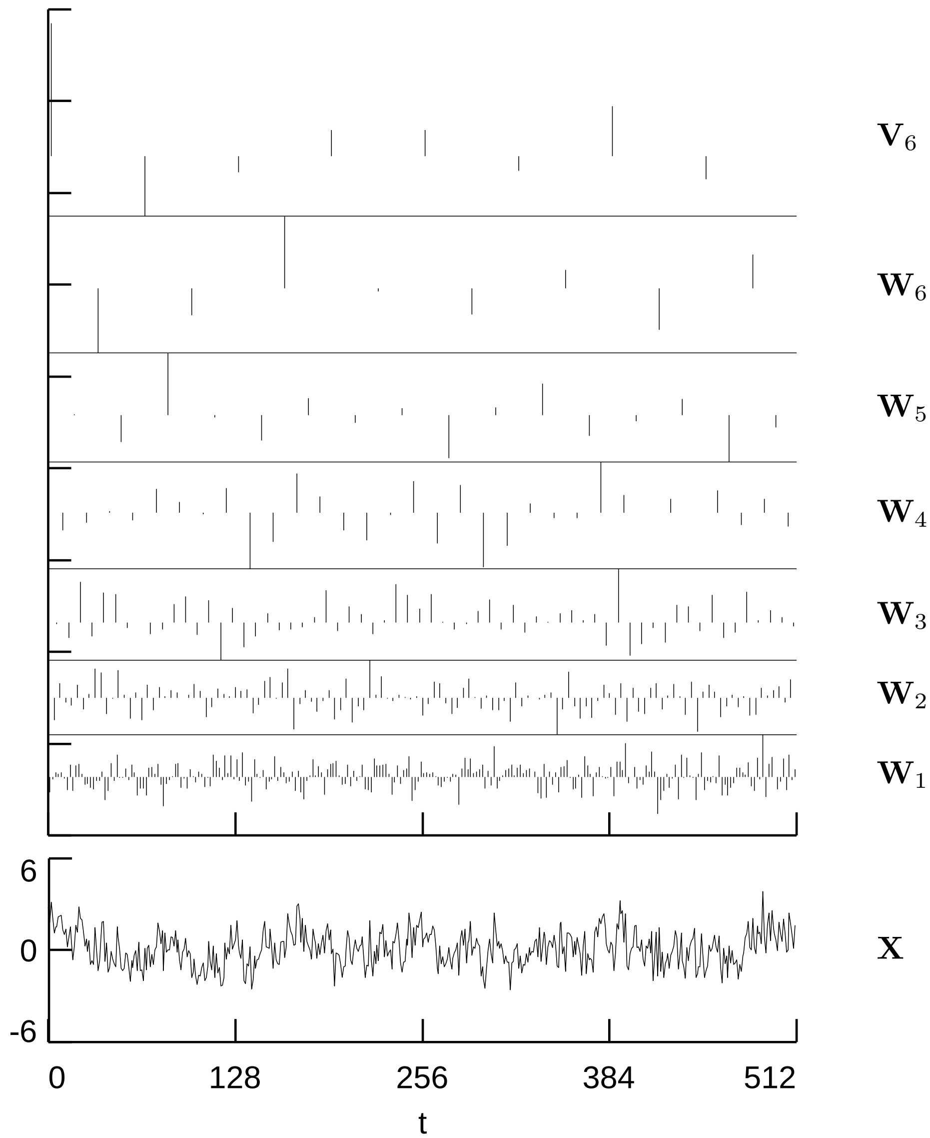


**Figure 1.** Simulated FDP(0.4) process of $N = 512$ points (bottom) and its DWT decomposition (top) using LA(8) wavelet filter.

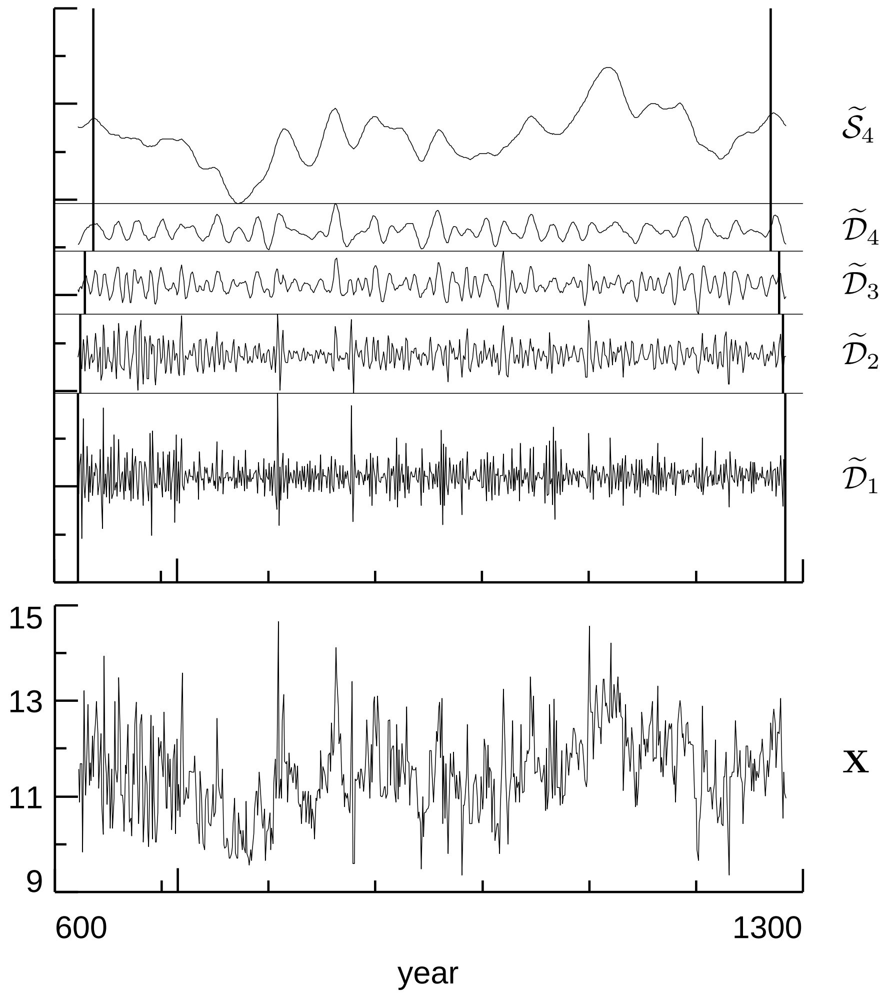


**Figure 2.** Level $J_0 = 4$ MODWT multiresolution analysis of Nile River minima (in meters) using the Haar wavelet filter.

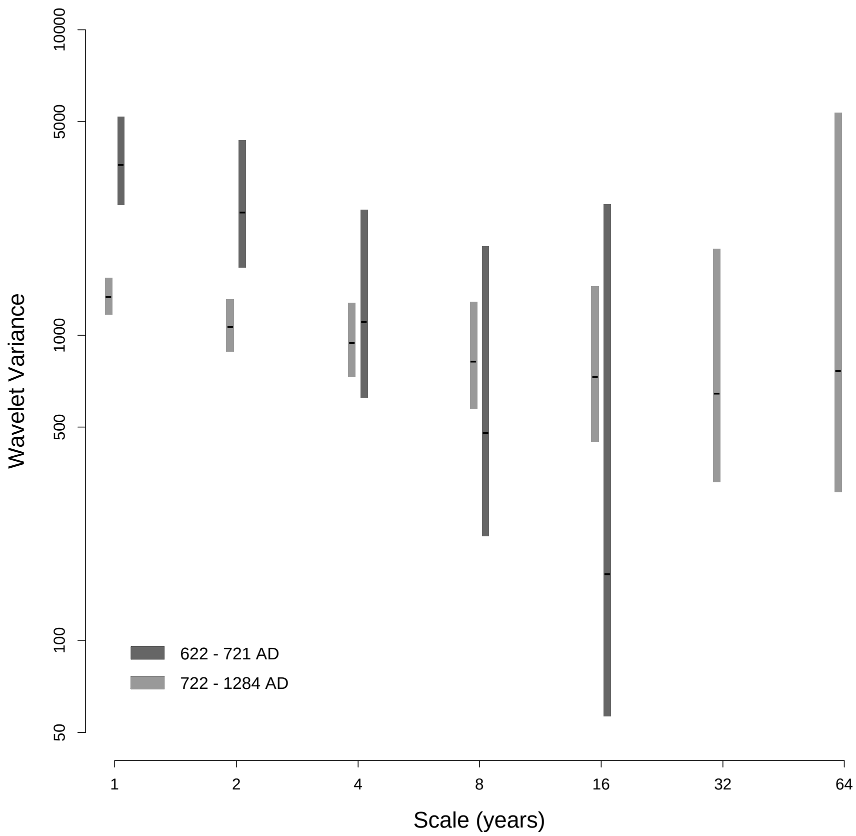


**Figure 3.** Estimated Haar wavelet variances for the Nile River minimum water levels before and after the year 721 AD, along with 95% confidence intervals based upon a chi-square approximation (Percival, 1995).

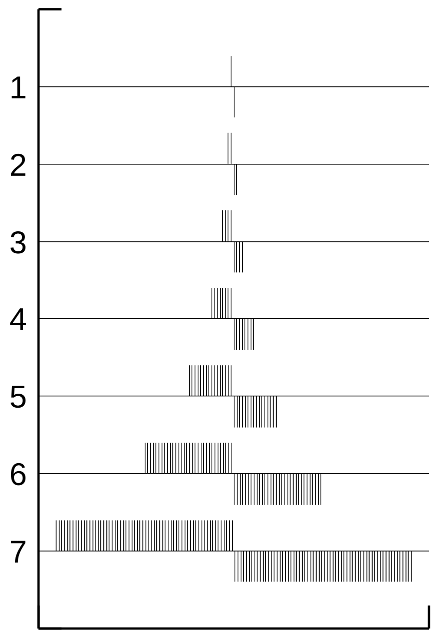


**Figure 4.** Haar wavelet filters for scales $\tau_j = 2^{j-1}$, $j = 1, 2, \ldots, 7$.

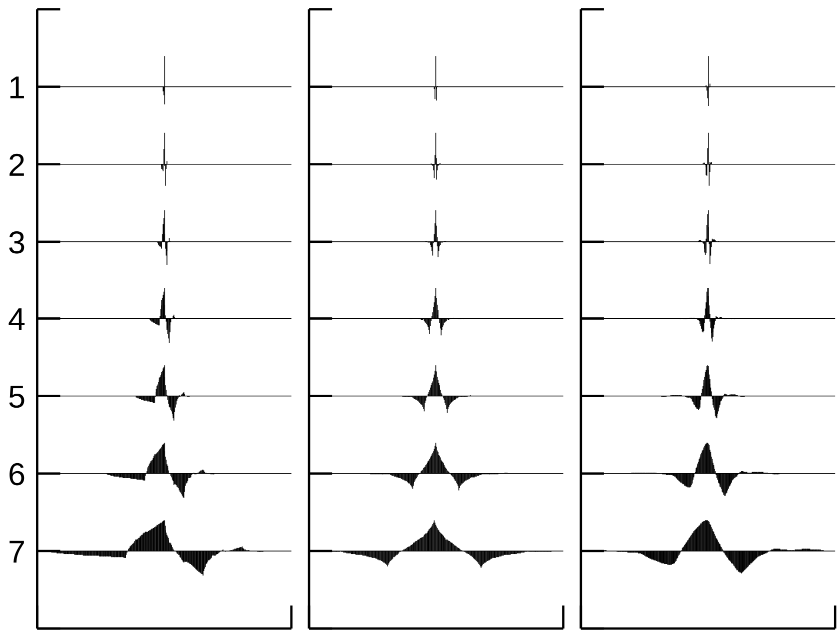


**Figure 5.** D(4), C(6) and LA(8) wavelet filters for scales $\tau_j = 2^{j-1}$, $j = 1, 2, \ldots, 7$.

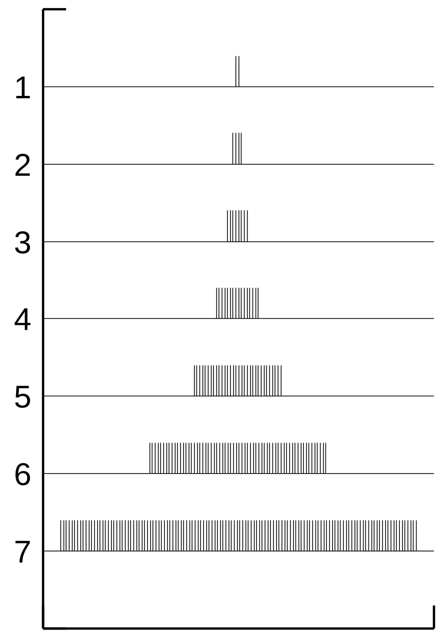


**Figure 6.** Haar scaling filters for scales $\lambda_j = 2^{J_0},\ J_0 = 1, 2, \ldots, 7$.

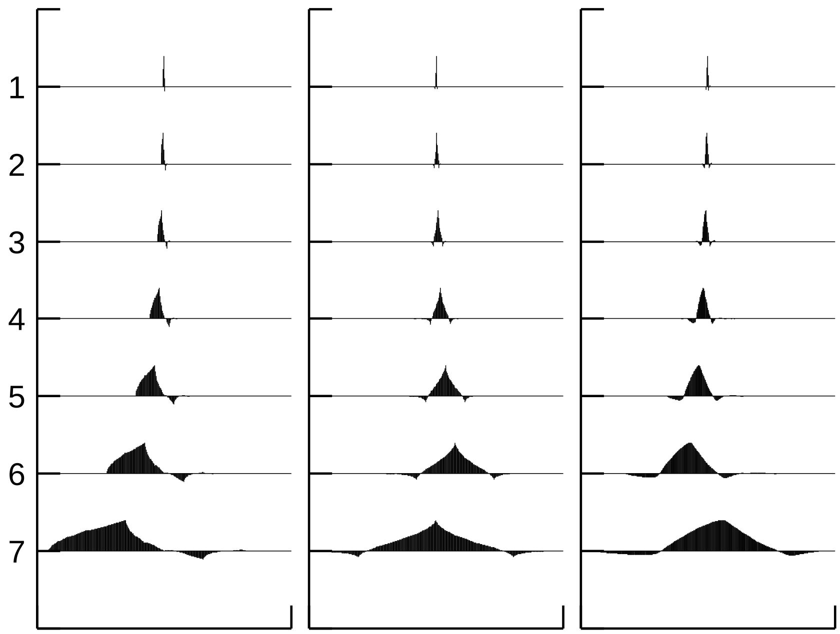


**Figure 7.** D(4), C(6) and LA(8) scaling filters for scales $\lambda_j = 2^{J_0}$, $J_0 = 1, 2, \ldots, 7$.

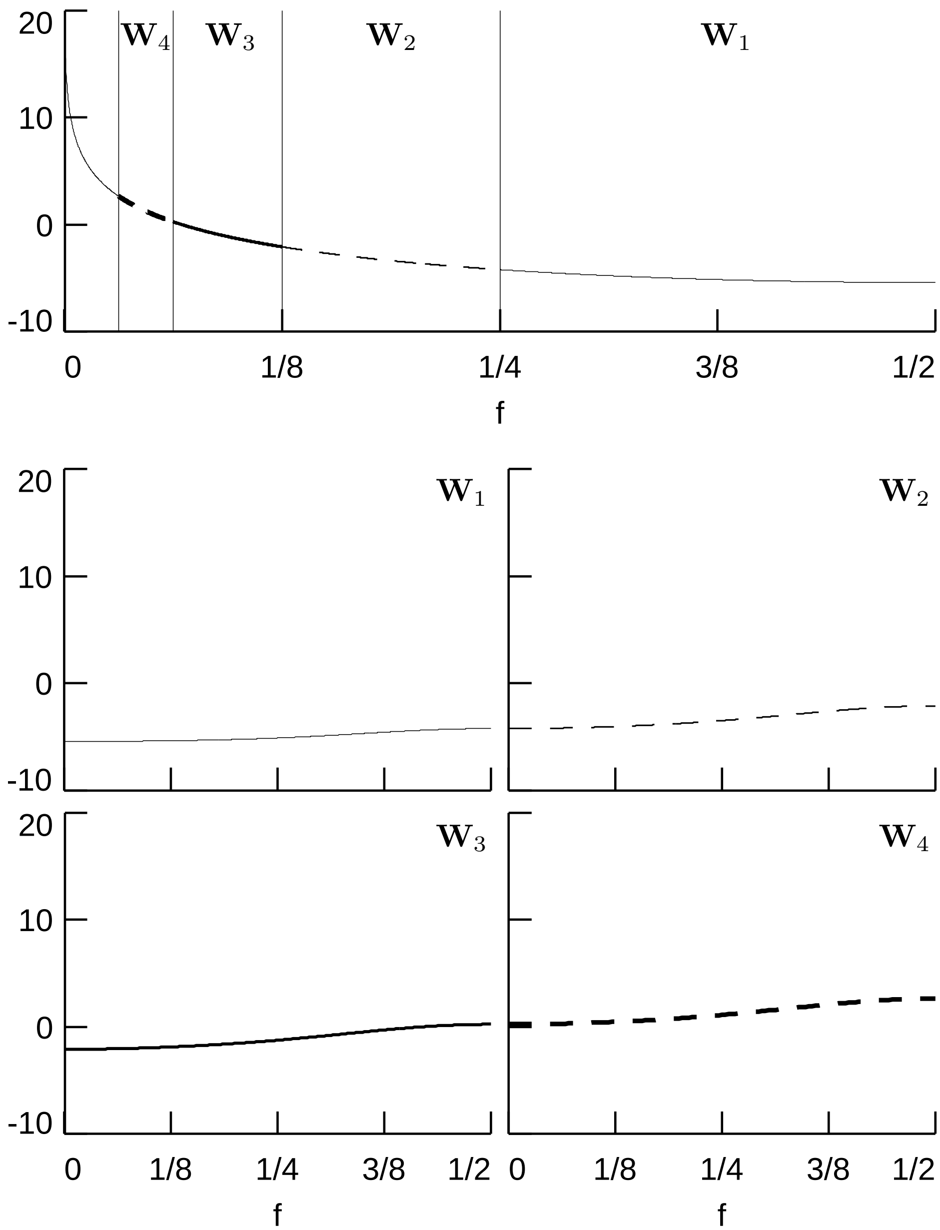


**Figure 8.** SDFs for FDP(0.4) process (top) and for LA(8) wavelet coefficients $\mathbf{W}_1$, $\mathbf{W}_2$, $\mathbf{W}_3$ and $\mathbf{W}_4$ (vertical axes are in measured in decibels).

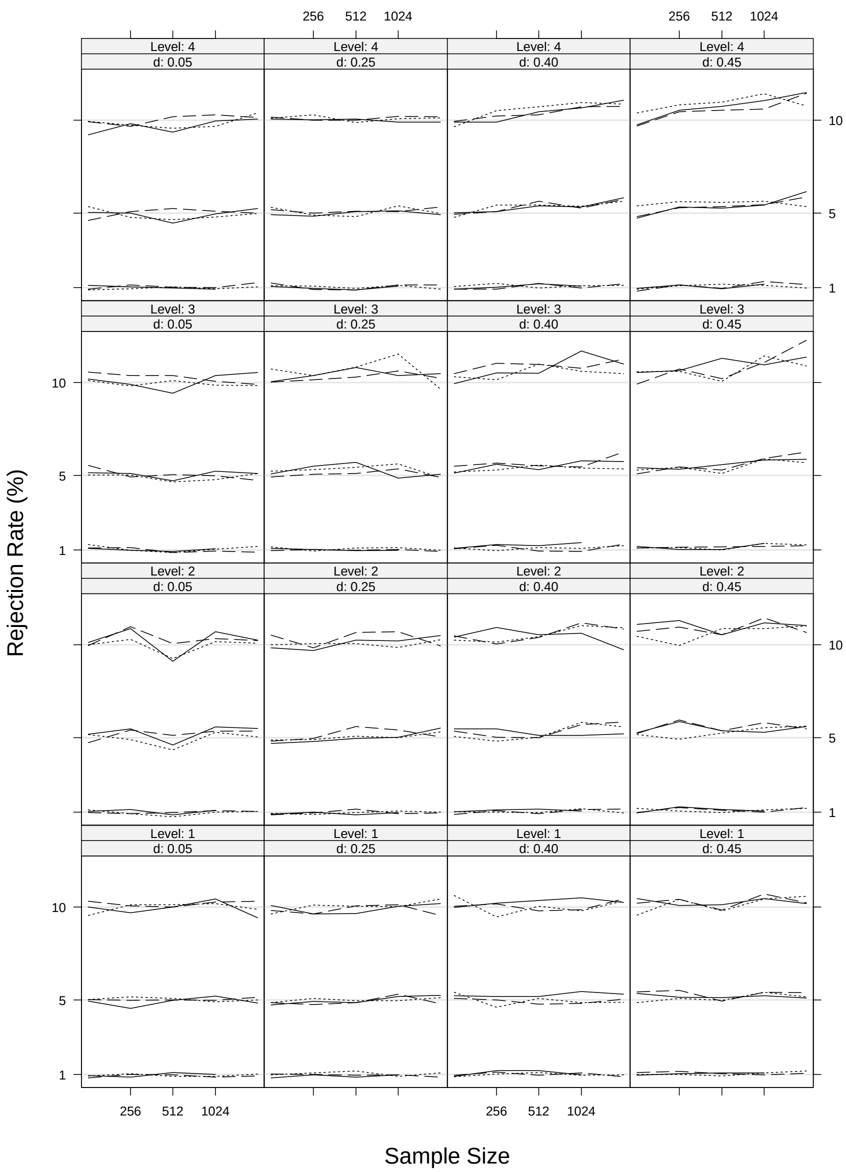


**Figure 9.** Rejection rates for FDPs using white noise critical levels, $N = 128$, 256, 512, 1024 and 2048. The solid line is the Haar wavelet filter, the dotted line is the D(4) and the dashed line is the LA(8). Each cell corresponds to a different combination of the level $j$ of the DWT and long memory parameter $d$. The rows correspond to – from bottom to top – levels 1, 2, 3 and 4, and the columns correspond to – from left to right – $d = 0.05$, 0.25, 0.40 and 0.45.

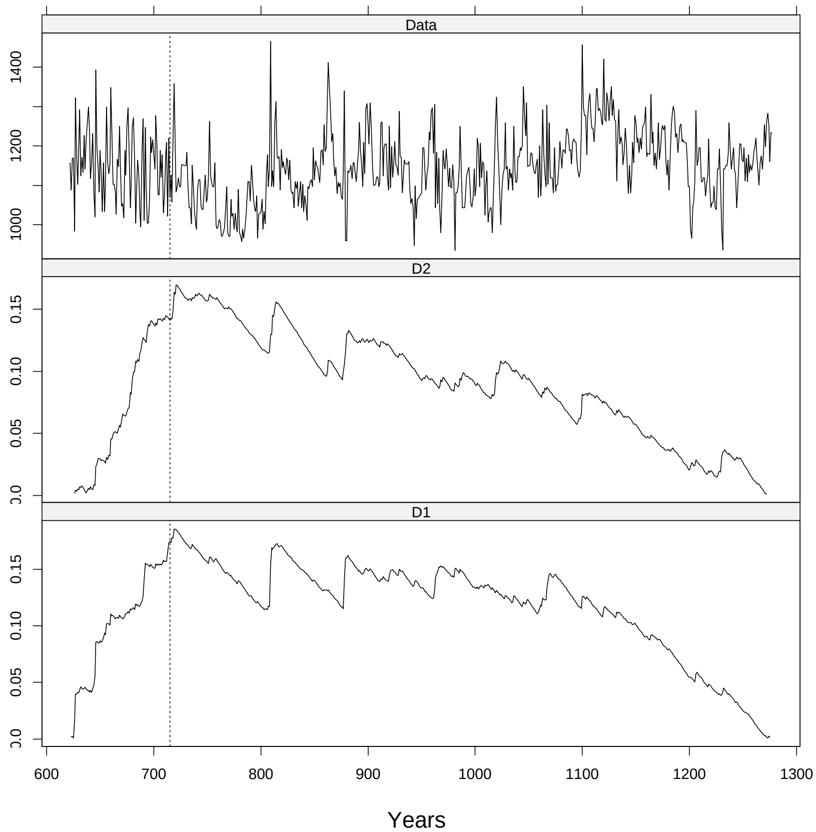


**Figure 10.** Normalized cumulative sum of squares from the MODWT, using the D(4) wavelet, for the Nile River minimum water levels. The dotted line marks the year 715 AD, when Nile River water levels began being recorded with a Nilometer constructed at Roda island.

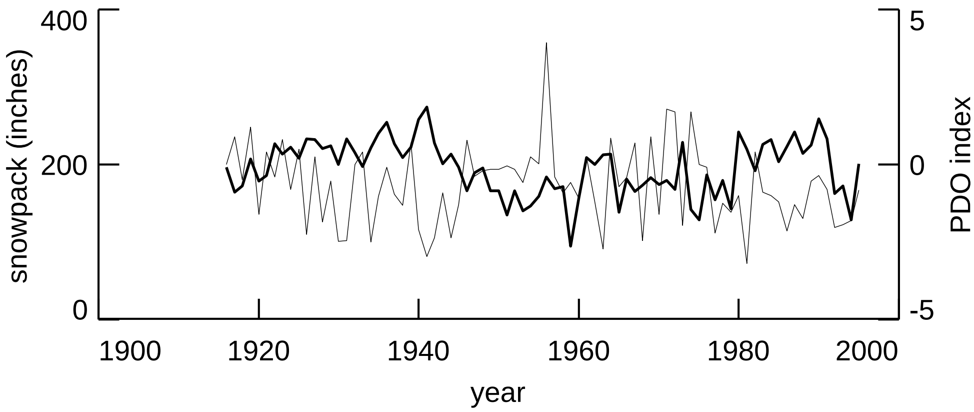


**Figure 11.** Pacific decadal oscillation (PDO) index $X_t$ (thick curve, right-hand axis) and March 15 snow depth at Paradise Ranger Station (1600 meters above sea level) on Mt. Rainer $Y_t$ (thin curve, left-hand axis). Both time series have one value per year from 1916 to 1996.

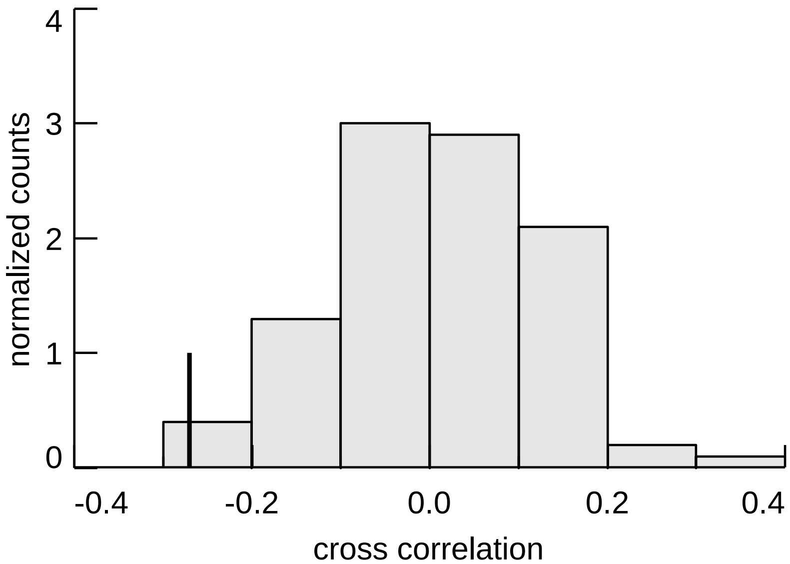


**Figure 12.** Histogram of bootstrapped cross-correlations to assess significance of $\hat{\rho}_0^{(XY)}$ computed for the two time series in Figure 11.

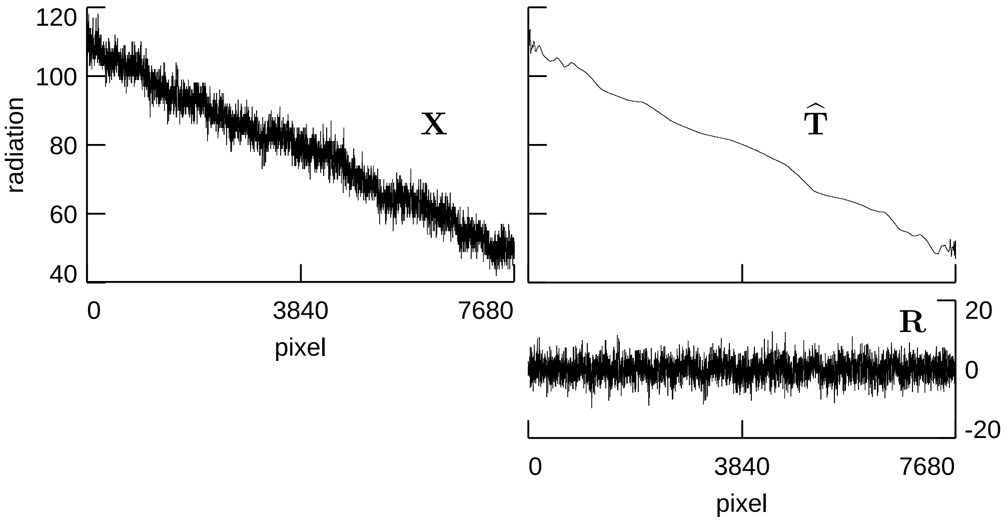


**Figure 13.** Decomposition of Honeywell uncooled microbolometer camera data into trend $\widehat{\mathbf{T}}$ and residuals $\mathbf{R} \equiv \mathbf{X} - \widehat{\mathbf{T}}$ (see Hewer *et al.*, 1994, for details about this atmospheric time series). The time series $\mathbf{X}$ consists of $N = 7680$ values, and we have used a $J_0 = 9$ partial DWT based upon the LA(8) wavelet filter (this filter is capable of handling polynomial trends up to order $r = 3$).